

## Quantum superconductor-insulator transition in titanium monoxide thin films with a wide range of oxygen contents

Y. J. Fan,<sup>1</sup> C. Ma,<sup>1</sup> T. Y. Wang,<sup>1,2</sup> C. Zhang,<sup>1</sup> Q. L. Chen,<sup>1</sup> X. Liu,<sup>1</sup> Z. Q. Wang,<sup>2</sup> Q. Li,<sup>2</sup> Y. W. Yin,<sup>1,\*</sup> and X. G. Li<sup>1,3,†</sup>

<sup>1</sup>Hefei National Laboratory for Physical Sciences at the Microscale, Department of Physics, and CAS Key Laboratory of Strongly-Coupled Quantum Matter Physics, University of Science and Technology of China, Hefei 230026, China

<sup>2</sup>Department of Physics, Pennsylvania State University, University Park, Pennsylvania 19019, USA

<sup>3</sup>Key Laboratory of Materials Physics, Institute of Solid State Physics, Hefei 230026, China and Collaborative Innovation Center of Advanced Microstructures, Nanjing 210093, China



(Received 1 April 2018; revised manuscript received 21 July 2018; published 7 August 2018)

The superconductor-insulator transition (SIT), one of the most fascinating quantum phase transitions, is closely related to the competition between superconductivity and carrier localization in disordered thin films. Here, superconducting  $\text{TiO}_x$  films with different oxygen contents were grown on  $\text{Al}_2\text{O}_3$  substrates by a pulsed laser deposition technique. The increasing oxygen content leads to an increase of disorder, a reduction of carrier density, an enhancement of carrier localization, and therefore a decrease of superconducting transition temperature. A fascinating SIT emerges in cubic  $\text{TiO}_x$  films with increasing oxygen content and its critical sheet resistance is close to the quantum resistance  $h/(2e)^2 \sim 6.45 \text{ k}\Omega$ . The scaling analyses of magnetic field–tuned SITs show that the critical exponent products  $z\nu$  increase from 1.02 to 1.31 with increasing disorder. Based on the results, the SIT can be described by the “dirty boson” model, and a schematic phase diagram for  $\text{TiO}_x$  films was constructed.

DOI: [10.1103/PhysRevB.98.064501](https://doi.org/10.1103/PhysRevB.98.064501)

### I. INTRODUCTION

Superconductor-insulator transition (SIT), as one fascinating example of quantum phase transitions [1], has remained an active topic in recent years. The SIT could be controlled by various nonthermal tuning parameters [2], including disorder [3–6], thickness [7–9], magnetic field [4,7,10,11], chemical composition [12,13], carrier density [4,14], and gate voltage [15,16] in two-dimensional (2D) superconductors. Taking disorder as an example, for the disorder strength below a critical transition value, the film is in a superconducting state characterized by the superconducting electron-pair wave function with a nonzero amplitude and a time-independent coherent phase. With the disorder close to the critical value, the system enters the critical regime where excitations (such as electrons and vortices) are strongly correlated. In the high disorder regime exceeding the critical value, the system is insulating. Theoretically, SIT can be achieved by either the phase or amplitude fluctuations [2,17], due to two different mechanisms. One is the bosonic model [18], where the SIT appears in the presence of the phase fluctuations. In this framework, the superconducting phase corresponds to a condensate of Cooper pairs with localized vortices, while an insulating phase corresponds to a condensate of vortices with localized Cooper pairs. The other one is a fermionic description [19] where, in the insulating phase, the Cooper pairs are broken into individually localized electrons corresponding to the amplitude fluctuations. Despite the efforts for investigating the SIT over

the last few decades, there are still many open issues, for example, the appearance of a metallic intermediate phase between the superconducting and insulating phases [7,10], different critical exponents signifying different universality classes [7,10,11,20], and various values of critical transition points found in different materials [4,8,9,21]. To clarify these issues and explore more interesting phenomena, researchers are still looking for new SIT systems with widely tunable parameters, as recently reported in the  $\text{LaAlO}_3/\text{SrTiO}_3$  interface [22] and  $\text{NbSe}_2$  monolayer [23].

Recently, epitaxial titanium monoxide  $\text{TiO}_x$  films were discovered to display enhanced superconductivity ( $T_c \sim 7.4 \text{ K}$ ) [24,25], compared with its polycrystalline bulk form ( $T_c \sim 5.5 \text{ K}$ ) [26]. One of the most interesting properties of  $\text{TiO}_x$  is that its oxygen content can be tuned in a significantly wide range  $0.7 < x < 1.3$  without changing its cubic structure [27], and the superconducting state with the maximum  $T_c$  was observed at  $x \sim 1.05$  in bulk  $\text{TiO}_x$  [28]. As demonstrated by a thermodynamic model, the minimum strength of the structural disorder also occurs at  $x \sim 1.05$  [29]. Namely, the stronger the disorder is, the lower the  $T_c$  would be. Considering that the increasing disorder may induce an SIT,  $\text{TiO}_x$  with widely tunable oxygen contents and disorder strengths, in which SIT has not been observed yet, may provide an ideal platform to study the nature of SIT.

In this paper, we found that, with increasing oxygen content in  $\text{TiO}_x$  ( $1.08 \leq x \leq 1.28$ ) films, the disorder and carrier localization enhance, while the carrier density decreases, and thus the superconducting transition temperature decreases. Importantly,  $\text{TiO}_x$  films display both oxygen content– and magnetic field–tuned SIT, which can be described by the dirty bosonic model. A schematic phase diagram for disordered  $\text{TiO}_x$  films was constructed accordingly.

\*Corresponding author: [yyw@ustc.edu.cn](mailto:yyw@ustc.edu.cn)

†Corresponding author: [lixg@ustc.edu.cn](mailto:lixg@ustc.edu.cn)

## II. EXPERIMENT

TiO<sub>x</sub> epitaxial films with thicknesses of 70–80 nm were grown on (0001)-oriented  $\alpha$ -Al<sub>2</sub>O<sub>3</sub> single crystalline substrates by a pulsed laser deposition technique under different oxygen pressures  $P_{O_2}$  as  $6 \times 10^{-4}$  Pa (labeled as P-6),  $6.5 \times 10^{-4}$  Pa (P-6.5),  $7 \times 10^{-4}$  Pa (P-7),  $7.5 \times 10^{-4}$  Pa (P-7.5),  $8 \times 10^{-4}$  Pa (P-8),  $8.5 \times 10^{-4}$  Pa (P-8.5), and  $9 \times 10^{-4}$  Pa (P-9), respectively. The crystal structure, chemical composition, and film thickness of representative samples were characterized by x-ray diffraction, electron energy-loss spectroscopy, and cross-sectional scanning electron microscopy, respectively, as shown in the Supplemental Material, Figs. S1 and S2 [30]. A Hall bar geometry was used to perform the resistivity and the Hall measurements. The transport measurements in magnetic field were carried out in a Physical Property Measurement System (PPMS-9T, Quantum Design) down to 0.45 K, while the resistivity vs temperature measurements in zero magnetic field down to 0.05 K were performed in a dilution refrigerator.

## III. RESULTS AND DISCUSSION

### A. Oxygen content- and magnetic field-tuned SIT

Figure 1 shows the temperature-dependent resistivities ( $\rho$ - $T$ ) for the TiO<sub>x</sub> films (P-6, P-6.5, P-7, P-7.5, P-8, P-8.5, and P-9). One can see that the resistivity increases with increasing oxygen content. The right inset of Fig. 1 displays the superconducting transition and the sheet resistance  $R_{\square}$  (resistance per square  $R_{\square} = \rho/d = RW/L$ , where  $d$  is thickness,  $W$  is width, and  $L$  is length) with an enlarged view at low temperatures. The

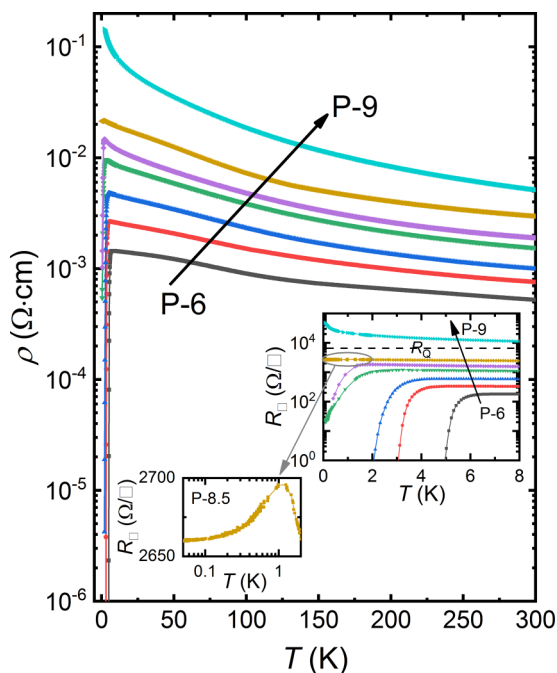


FIG. 1. Temperature-dependent resistivities for TiO<sub>x</sub> films (P-6, P-6.5, P-7, P-7.5, P-8, P-8.5, and P-9). Right inset: The enlarged view of sheet resistances for TiO<sub>x</sub> films at low temperatures, and the critical quantum resistance  $R_Q = 6.45$  k $\Omega$ . Left inset: The gray open circle and arrow correspond to the enlarged sheet resistance of P-8.5 below 2 K.

cubic TiO<sub>x</sub> films with  $1.08 \leq x \leq 1.19$  are superconductors with the onset superconducting transition temperature  $T_{c,\text{onset}}$  (defined by the resistivity dropping to 90% of the normal state resistivity) gradually decreasing from 6.12 K for P-6 to 1.08 K for P-8.5. At an even higher oxygen content,  $x = 1.28$  (P-9), the TiO<sub>x</sub> film becomes a non-superconducting insulator. This implies that a clear oxygen content-driven SIT appears in TiO<sub>x</sub> films. Close to the  $T = 0$  K limit, a metallic intermediate phase [31] with the resistance saturating at a nonzero value appears between the superconducting and insulating phases, such as the P-8.5 specimen (see the left inset of Fig. 1). Thus, it would be more appropriate to describe the transition as a superconductor-metal-insulator transition. The similar intervening metallic phase with substantial superconducting fluctuations was also observed in Ta [7] and MoGe [10], but not in TiN [6], which may be related to the different disorder strengths [20,32]. The critical transition sheet resistance for the SIT at zero temperature and zero magnetic field is close to the quantum sheet resistance  $R_Q \sim h/(2e)^2$  for Cooper pairs. This value is compatible with the prediction of the “dirty boson” model [33], which is valid at very low temperature when only Cooper pairs are present. It is also observed that the sheet resistance remains near  $R_Q$  upon increasing the temperature to high temperature  $T = 8$  K for sample P-8.5, where no Cooper pairs are expected. This behavior is not well understood at this point, and thus further theoretical and experimental investigations on the SIT are required.

Tuning the magnetic field across the putative quantum critical point allows one to investigate the critical scaling behavior in its vicinity. The SIT driven by magnetic field in samples P-7.5, P-8, and P-8.5 shows that the magnetoresistance isotherms cross at a characteristic value of magnetic field  $H_c$ , as depicted in the left panels of Fig. 2. The approximate values for  $H_c$  and  $R_c$  are marked with the red arrows. Here,  $R_c$  is the temperature-independent critical resistance at the transition point. For  $H < H_c$ , the samples are in a superconducting state, and the sheet resistance  $R_{\square}$  decreases with decreasing temperature. Approaching  $H_c$ , there is a diverging correlation length  $\xi \sim |H - H_c|^{-\nu}$ , and the characteristic frequency vanishes as  $\Omega \sim \xi^{-z}$ , where  $\nu$  is the static critical exponent of the correlation length and  $z$  is the dynamic critical exponent. The sheet resistance  $R_{\square}$  obeys a universal scaling law given by [1]

$$R_{\square}(H, T) = R_c f(|H - H_c|/T^{1/z\nu}), \quad (1)$$

where  $f(x)$  is a universal scaling function with a unique constraint:  $f(0) = 1$ . The right panels of Fig. 2 show the scalings near the SIT over a range of temperatures, and the critical exponent products  $z\nu$  are about 1.02 for P-7.5, 1.17 for P-8, and 1.31 for P-8.5, determined by evaluating the inverse slope of the log-log plot of  $(dR/dH)|_{H_c}$  vs  $1/T$  [11], as shown in the insets. Generally, considering a long-range Coulomb interaction among charges, the dynamical exponent  $z$  is found to be  $\sim 1$  [34]. According to the Harris criterion [35], the critical exponent  $\nu$  is less than 1 in a clean limit system, and in a disordered system (in the dirty regime),  $\nu$  is expected to over 1, as recently observed in superconducting LaTiO<sub>3</sub>/SrTiO<sub>3</sub> interfaces [36]. The relationship between the disorder and the critical exponent was also reported in InO<sub>x</sub> [11,20], which shows  $z\nu \sim 1.3$  and 2.3 for weakly and highly disordered states, respectively. In our case, the critical exponent

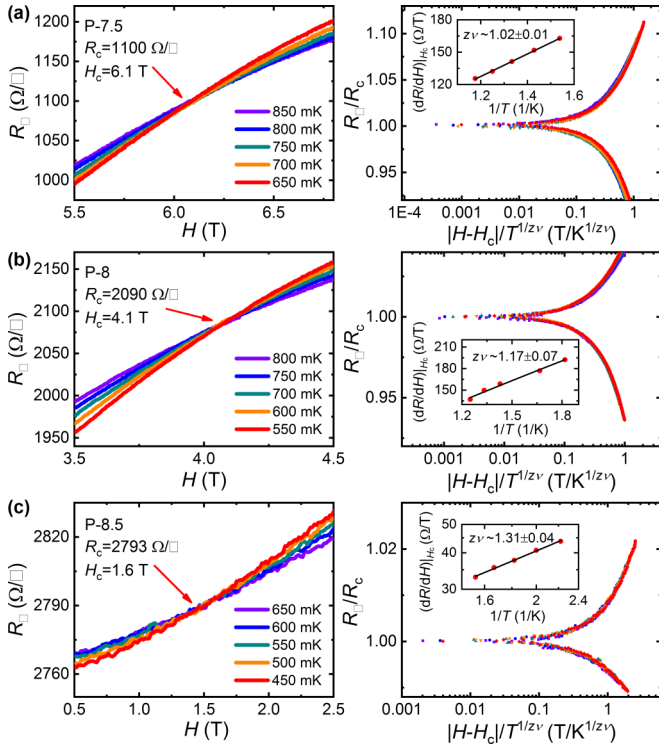


FIG. 2. Scaling behaviors of magnetic field-tuned SIT in  $\text{TiO}_x$  films: (a) P-7.5, (b) P-8, and (c) P-8.5. Left panels: Magnetoresistance isotherms for samples P-7.5, P-8, and P-8.5 near the SIT. Right panels: The scaling analysis corresponding to the left panels. Insets: The fitting results of a power law to the inverse temperature-dependent  $dR/dH$  at  $H_c$ .

products  $z\nu$  are 1.02 for P-7.5, 1.17 for P-8, and 1.31 for P-8.5, all larger than 1, consistent with the theoretical prediction in the “dirty boson” model [18], and the larger  $z\nu$  for the films with higher oxygen content is consistent with the enhanced disorder with increasing oxygen content.

Most SITs are experimentally observed and theoretically described in 2D thin films with their thicknesses smaller than or comparable to the superconducting coherence lengths  $\xi(0)$  at zero temperature [37]. To check the  $\xi(0)$  values of the  $\text{TiO}_x$  samples, we studied the superconductivity for higher-transition-temperature samples (P-6, P-6.5, and P-7) in magnetic fields. Figures 3(a) and 3(b) show the temperature-dependent resistivities of a typical  $\text{TiO}_x$  film, P-7, in different magnetic fields (0, 0.5, 1, 3, 5, 7, 9 T) with both perpendicular [ $H \perp(111)$ ] and parallel [ $H \parallel(111)$ ] fields. With increasing magnetic field, the resistivity broadening becomes slightly wider and the onset of superconductivity gradually shifts to a lower temperature. Figure 3(c) shows the temperature dependence of the upper critical field  $H_{c2}(T)$  (defined by the resistivity drop at 90% of the normal state resistivity [38]), which can be well fitted by the Werthamer-Helfand-Hohenberg (WHH) theory [39]. Similar results for P-6 and P-6.5 were also obtained, as shown in Fig. S3 [30]. We summarized the  $H_{c2}(0)$  and fitting parameters for P-6, P-6.5, and P-7 in Fig. 3(d), indicating that the strong disorder may contribute to the spin-paramagnetic effect, and cause a large  $\alpha$  at high oxygen content [40,41]. The details for the variations of

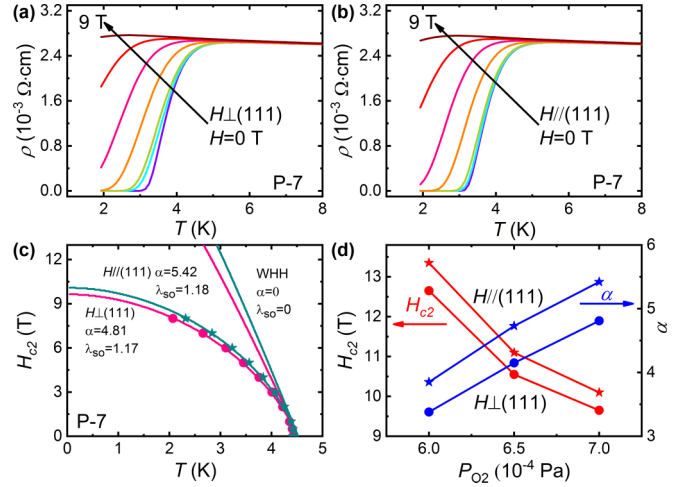


FIG. 3. (a,b) Temperature-dependent resistivities of P-7 in magnetic fields for  $H \perp(111)$  and  $H \parallel(111)$  from 0 to 9 T (0, 0.5, 1, 3, 5, 7, and 9 T), respectively. (c) Temperature-dependent  $H_{c2}(T)$  of P-7 for  $H \perp(111)$  (closed circles) and  $H \parallel(111)$  (closed stars). Solid lines are the fitting curves with the WHH model. (d)  $P_{\text{O}_2}$ -dependent  $H_{c2}(0)$  (red symbol lines) and  $\alpha$  (blue symbol lines) for  $H \perp(111)$  (closed circles) and  $H \parallel(111)$  (closed stars).

$H_{c2}(T)$  with temperature and oxygen content are discussed in the Supplemental Material, S2: Upper critical fields [30]. According to the equation  $\xi(0) = [\varphi_0/2\pi H_{c2}(0)]^{1/2}$  where  $\varphi_0$  is the flux quantum, we can obtain the superconducting coherence lengths  $\xi(0)$  as 5.1, 5.6, and 5.8 nm for samples P-6, P-6.5, and P-7, respectively. On the other hand, another important superconductivity related physical length scale, the London penetration depth  $\lambda(0)$ , is about 670.7 nm for a TiO film ( $\sim 80$  nm), as obtained in our previous report [25]. Thus, we can see that the thicknesses (70–80 nm) of our samples are longer than the coherence length  $\xi(0)$  but much shorter than the penetration depth. In spite of this, the SIT behavior still appears in  $\text{TiO}_x$  films and could be described by a 2D scaling theory.

In fact, it is still controversial whether a 2D theory of superconductivity cannot be used for a thick film. For example, the magnetic field-induced fluctuating conductivity around transition temperature in superconducting MoGe with a thickness of 69 nm [42], the vortex-glass transition in superconducting TiO with thickness of 80 nm [25], and especially the magnetic field-tuned SIT in a superconducting  $\text{Mo}_3\text{Si}$  film with thickness of 170 nm [43], have been successfully described by the 2D theory of superconductivity, although their thicknesses (much longer than superconducting coherence length) make them more like a three-dimensional (3D) system. Thus, maybe sometimes the 2D SIT behavior could be observed in a certain thick film, or a 2D theory may be extended to a 3D system to describe the superconductivity in a certain thick film. It has been demonstrated theoretically that sometimes the SIT scenarios are very similar in 2D and 3D systems [44]. This is an open issue and deserves further investigations.

## B. First-principles calculation of electronic structure

It is well known that the electric transport properties of materials, including the superconducting properties, are

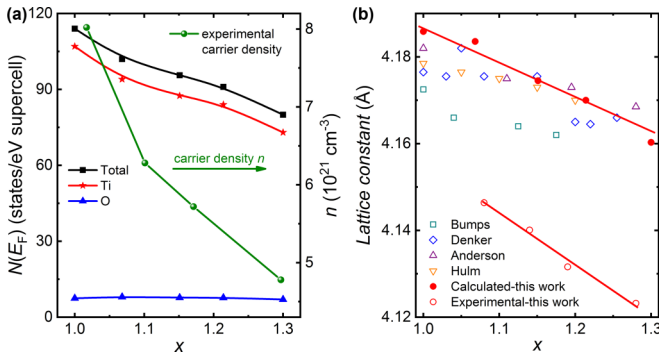


FIG. 4. (a) Oxygen content  $x$ -dependent total and partial DOS  $N(E_F)$  at the Fermi level of  $\text{TiO}_x$ . Experimental values of the carrier density of  $\text{TiO}_x$  films as a function of oxygen content  $x$ . (b) Lattice parameters  $a$  from the theoretical calculation, experimental data, and reference values of  $\text{TiO}_x$  as a function of oxygen content  $x$ . Open symbols are experimental data, and solid symbols are calculated values.

closely related to the electron density of states (DOS) at the Fermi level which can be obtained by theoretical calculation of the electronic structures [45]. Here, the electronic structures of  $\text{TiO}_x$  with different oxygen contents were calculated by a supercell method with density functional theory (DFT) [46,47]. A  $3 \times 3 \times 3$  supercell of  $\text{TiO}$  based on the optimized cell was created to act as the computational model (see detailed description in the Supplemental Material, S3: First-principles calculation of density of states and lattice constant of  $\text{TiO}_x$  [30]).  $\text{TiO}_x$  contains a certain amount of both titanium and oxygen vacancies. The increase of oxygen content corresponds to an increase (a decrease) of the vacancy concentration in the titanium (oxygen) sublattice [29]. The detailed calculation results are illustrated in Fig. S6 in the Supplemental Material [30]. We found that the total electron DOS  $N(E_F)$  at the Fermi level of  $\text{TiO}_x$  ( $x$  from 1 to 1.3) is mainly derived from  $d$  states of titanium atoms, and it decreases with the increase of titanium vacancies, as shown in Fig. 4(a). The decrease of  $N(E_F)$  indicates the decrease of carrier density, and thus the increase of resistivity as well as the decrease of superconducting transition temperature as a result. This is consistent with the Hall measurements showing that the room temperature electron density  $n$  decreases with increasing oxygen content, as shown in Figs. 4(a) and Fig. S7 in the Supplemental Material [30]. It is also confirmed that the  $n$ -type electronic charge carriers dominate the conduction mechanism. Furthermore, Fig. 4(b) shows that the calculated lattice parameter  $a$  decreases with increasing oxygen content. The red line is drawn through the solid circles calculated in the present work, consistent with the earlier experiment results (the open symbols) in bulk  $\text{TiO}_x$  [28]. The experimental values (red open circles) in  $\text{TiO}_x$  films are less than the values of bulk, which may be due to the substrate strain on films.

### C. Localization length

Usually, the superconductivity of a material is closely connected with the physical properties in its normal state, such as the disorder strength and electron localization length, which could be obtained by quantitative analyses of trans-

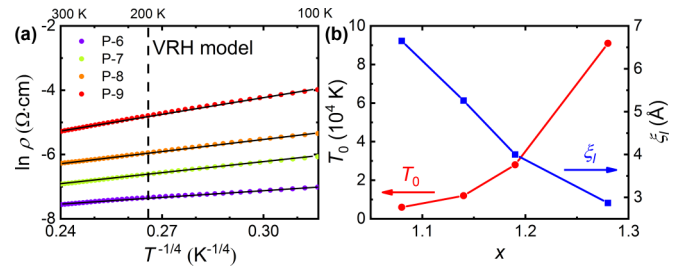


FIG. 5. (a) The fitting results of  $\rho$ - $T$  curves with the VRH model for  $\text{TiO}_x$  films (P-6, P-7, P-8, and P-9) in the temperature range from 300 to 100 K. The points are the experimental values, and the black lines represent the fitting results. (b) Oxygen content  $x$ -dependent on the characteristic temperature  $T_0$  and localization length  $\xi_l$  in  $\text{TiO}_x$ .

port behaviors in the normal state [48,49]. Thus, we used the variable range hopping (VRH) model [50] to fit the normal state  $\rho$ - $T$  curves of  $\text{TiO}_x$  films (P-6, P-7, P-8, P-9) from 300 to 100 K. Figure 5(a) shows the fitting results with  $\rho(T) = \rho_0 \exp(T_0/T)^{1/4}$ . Here, the characteristic temperature  $T_0$  is given by  $T_0 = 24/[\pi k_B N(E_F) \xi_l^3]$ , where  $\xi_l$  is the localization length. The fitted values of  $T_0$  are  $0.6 \times 10^4 \text{ K}$  for P-6,  $1.2 \times 10^4 \text{ K}$  for P-7,  $2.8 \times 10^4 \text{ K}$  for P-8, and  $9.1 \times 10^4 \text{ K}$  for P-9. According to the calculated lattice parameters and  $N(E_F)$  in a  $3 \times 3 \times 3$  supercell, the  $N(E_F)$  values are about  $5.07 \times 10^{28} \text{ eV}^{-1} \text{ m}^{-3}$ ,  $4.89 \times 10^{28} \text{ eV}^{-1} \text{ m}^{-3}$ ,  $4.69 \times 10^{28} \text{ eV}^{-1} \text{ m}^{-3}$ , and  $4.21 \times 10^{28} \text{ eV}^{-1} \text{ m}^{-3}$  for P-6, P-7, P-8, and P-9, respectively. Based on the values of  $T_0$  and  $N(E_F)$ , we can obtain

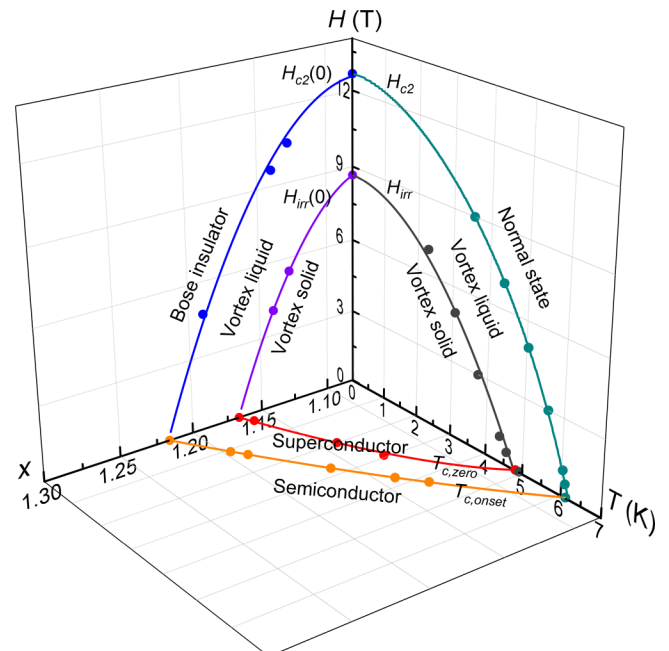


FIG. 6. Schematic phase diagram of  $\text{TiO}_x$  films for oxygen content ( $x$ ), magnetic field ( $H$ ) and temperature ( $T$ ). The points are the experimental values. The WHH theory and an empirical equation  $H_{irr}(T) = H_{irr}(0)[1 - (T/T_{c,zero})^2]$  [where  $H_{irr}(0)$  is the irreversibility field at absolute zero temperature] are used to fit the temperature-dependent  $H_{c2}$  and  $H_{irr}$ , respectively. Other solid lines are quadratic fitting curves. The different regimes of the diagram are described in the text.

TABLE I. Structural and electronic properties of representative  $\text{TiO}_x$  films (P-6, P-7, P-8, and P-9), including the stoichiometry  $x$ , thickness  $d$ , superconducting transition temperature  $T_{c,\text{onset}}$ , room-temperature resistivity  $\rho$ , upper critical field  $H_{c2}(0)$ , coherence length  $\xi(0)$ , localization length  $\xi_l$ , electron density of states at the Fermi level  $N(E_F)$ , and carrier density  $n$ .

Sample name	$x$ ( $\text{TiO}_x$ )	$d$ (nm)	$T_{c,\text{onset}}$ (K)	$\rho$ (300 K) ( $\Omega \text{ cm}$ )	$H_{c2}(0)$ (T)	$\xi(0)$ (nm)	$\xi_l$ ( $\text{\AA}$ )	$N(E_F)$ ( $\text{eV}^{-1} \text{ m}^{-3}$ )	$n$ ( $10^{21} \text{ cm}^{-3}$ )
P-6	1.08	80	6.12	$5.2 \times 10^{-4}$	12.7	5.1	6.65	$5.07 \times 10^{28}$	8.02
P-7	1.14	77	3.72	$9.9 \times 10^{-4}$	9.6	5.8	5.26	$4.89 \times 10^{28}$	6.28
P-8	1.19	74	1.37	$1.9 \times 10^{-3}$	4.7	8.4	4.00	$4.69 \times 10^{28}$	5.72
P-9	1.28	73	N/A	$5.1 \times 10^{-3}$	N/A	N/A	2.87	$4.21 \times 10^{28}$	4.78

the values of  $\xi_l$  which are 6.65, 5.26, 4.00, and 2.87  $\text{\AA}$ , respectively, as shown in Fig. 5(b). With oxygen content  $x$  from 1.08 to 1.28, the decreased  $\xi_l$  contributes 12.6 times the increase of  $T_0$ , much larger than the contribution of the decreased  $N(E_F)$  (about 20%). It is clear that the decreases of  $\xi_l$  can inevitably localize the Cooper pairs [48], and thus reduce the superconducting transition temperature significantly at high oxygen content. The enhanced carrier localization also reflects the increase of disorder [51,52] at high oxygen content.

#### D. Superconductor-insulator phase diagram

In order to obtain a comprehensive understanding of the quantum SIT in  $\text{TiO}_x$  films driven by both oxygen content and magnetic field, a superconductor-insulator phase diagram was constructed with different magnetic fields, temperatures, and oxygen contents, as shown in Fig. 6, and the physical parameters for representative samples (P-6, P-7, P-8, and P-9) are summarized in Table I. In the phase diagram, the  $H_{c2}$  and  $T_{c,\text{onset}}$  lines separate the superconducting state and the normal state. The  $T_{c,\text{zero}}$  is defined by the resistivity dropping to zero. The irreversible field  $H_{\text{irr}}$ , defined as the field where the resistivity drops to 0.1% of the normal state resistivity [53], will further divide the superconducting phase into vortex solid and liquid phases [54–57]. At the  $T = 0 \text{ K}$  limit, with increasing oxygen content or magnetic field, the  $\text{TiO}_x$  film passes through the vortex solid, vortex liquid, Bose insulator, and Fermi insulator phases. Below  $H_{\text{irr}}(0)$ , the vortex solid phase mainly contains the condensate Cooper pairs and localized vortices [18]. According to Mulligan and Raghun's suggestion, the vortex liquid phase between  $H_{\text{irr}}(0)$  and  $H_{c2}(0)$  is a composite fermion metal, where composite fermions are mobile vortices attached to one flux quantum of an emergent gauge field [32]. Across  $H_{c2}(0)$ , the Bose insulating phase appears. In other words, the superconductor-metal and metal-insulator transitions occur around  $H_{\text{irr}}(0)$  and  $H_{c2}(0)$ , respectively. During the SIT driven by either oxygen content or magnetic field, the Cooper pairs are localized, and the vortices are delocalized and will undergo a Bose condensation [18,32,58]. With further increasing oxygen content or magnetic field,

the localized Cooper pairs are destroyed and the individual electrons are presumably localized. Inferred from the oxygen content-dependent superconducting transition temperatures of  $\text{TiO}_x$  films, at zero temperature and zero magnetic field, the critical oxygen contents are about 1.17 for superconductor-metal transition and 1.22 for metal-insulator transition, and with oxygen contents in between 1.17 and 1.22,  $\text{TiO}_x$  is in a metallic phase with a finite resistance.

#### IV. CONCLUSIONS

In summary, the effects of oxygen content on the superconductivity of  $\text{TiO}_x$  films were systematically investigated. With increasing oxygen content, the enhanced disorder and carrier localization as well as the decreased carrier density lead to the increase of resistivity, the decrease of superconducting transition temperature, and the appearance of SIT without changing the cubic structure of  $\text{TiO}_x$  films. The critical transition quantum resistance and the scaling behavior demonstrate that the SIT in  $\text{TiO}_x$  films follows a bosonic model, which illustrates that the appearance of the SIT is mainly due to the phase fluctuations induced by increasing oxygen content and magnetic field. A schematic phase diagram for disordered  $\text{TiO}_x$  films was constructed with three variables of magnetic field, temperature, and oxygen content.

#### ACKNOWLEDGMENTS

This work was supported by the Natural Science Foundation of China (Grants No. 51790491, No. 21521001, and No. 51622209) and by the National Basic Research Program of China (Grants No. 2016YFA0300103, No. 2015CB921201, and No. 2012CB922003). The work done at Penn State was supported by the United States Department of Energy under Grant No. DE-FG02-08ER46531 (Q.L.). The numerical calculations in this paper have been done on the supercomputing system in the Supercomputing Center of University of Science and Technology of China. Jue Jiang is acknowledged for his assistance in the extremely low temperature measurements.

Y.J.F. and C.M. contributed equally to this work.

[1] S. L. Sondhi, S. M. Girvin, J. P. Carini, and D. Shahar, *Rev. Mod. Phys.* **69**, 315 (1997).  
 [2] A. M. Goldman and N. Markovic, *Phys. Today* **51**(11), 39 (1998).  
 [3] S. V. Postolova, A. Y. Mironov, M. R. Baklanov, V. M. Vinokur, and T. I. Baturina, *Sci. Rep.* **7**, 1718 (2017).

[4] N. P. Breznay, M. Tendulkar, L. Zhang, S. C. Lee, and A. Kapitulnik, *Phys. Rev. B* **96**, 134522 (2017).  
 [5] B. Sacépé, C. Chapelier, T. I. Baturina, V. M. Vinokur, M. R. Baklanov, and M. Sanquer, *Phys. Rev. Lett.* **101**, 157006 (2008).

- [6] T. I. Baturina, A. Y. Mironov, V. M. Vinokur, M. R. Baklanov, and C. Strunk, *Phys. Rev. Lett.* **99**, 257003 (2007).
- [7] S. Y. Park, J. Shin, and E. Kim, *Sci. Rep.* **7**, 42969 (2017).
- [8] H. M. Jaeger, D. B. Haviland, B. G. Orr, and A. M. Goldman, *Phys. Rev. B* **40**, 182 (1989).
- [9] D. B. Haviland, Y. Liu, and A. M. Goldman, *Phys. Rev. Lett.* **62**, 2180 (1989).
- [10] A. Yazdani and A. Kapitulnik, *Phys. Rev. Lett.* **74**, 3037 (1995).
- [11] A. F. Hebard and M. A. Paalanen, *Phys. Rev. Lett.* **65**, 927 (1990).
- [12] S. Oh, T. A. Crane, D. J. Van Harlingen, and J. N. Eckstein, *Phys. Rev. Lett.* **96**, 107003 (2006).
- [13] Z. Z. Li, H. Rifi, A. Vaures, S. Megtert, and H. Raffy, *Phys. C (Amsterdam, Neth.)* **206**, 367 (1993).
- [14] Y. Saito, Y. C. Kasahara, J. T. Ye, Y. Iwasa, and T. Nojima, *Science* **350**, 409 (2015).
- [15] X. Leng, J. Garcia-Barriocanal, S. Bose, Y. Lee, and A. M. Goldman, *Phys. Rev. Lett.* **107**, 027001 (2011).
- [16] A. T. Bollinger, G. Dubuis, J. Yoon, D. Pavuna, J. Misewich, and I. Božović, *Nature* **472**, 458 (2011).
- [17] Y. Dubi, Y. Meir, and Y. Avishai, *Nature* **449**, 876 (2007).
- [18] M. P. A. Fisher, *Phys. Rev. Lett.* **65**, 923 (1990).
- [19] P. A. Lee and T. V. Ramakrishnan, *Rev. Mod. Phys.* **57**, 287 (1985).
- [20] M. A. Steiner, N. P. Breznay, and A. Kapitulnik, *Phys. Rev. B* **77**, 212501 (2008).
- [21] Y. Liu, D. B. Haviland, B. Nease, and A. M. Goldman, *Phys. Rev. B* **47**, 5931 (1993).
- [22] S. Shen, Y. Xing, P. Wang, H. Liu, H. Fu, Y. Zhang, L. He, X. C. Xie, X. Lin, J. Nie, and J. Wang, *Phys. Rev. B* **94**, 144517 (2016).
- [23] Y. Xing, K. Zhao, P. J. Shan, F. P. Zheng, Y. W. Zhang, H. L. Fu, Y. Liu, M. L. Tian, C. Y. Xi, and H. W. Liu, *Nano Lett.* **17**, 6802 (2017).
- [24] C. Zhang, F. X. Hao, G. Y. Gao, X. Liu, C. Ma, Y. Lin, Y. W. Yin, and X. G. Li, *npj Quantum Mater.* **2**, 2 (2017).
- [25] C. Zhang, F. X. Hao, X. Liu, Y. J. Fan, T. Y. Wang, Y. W. Yin, and X. G. Li, *Supercond. Sci. Technol.* **31**, 015016 (2018).
- [26] D. Wang, C. Huang, J. Q. He, X. L. Che, H. Zhang, and F. Q. Huang, *ACS Omega* **2**, 1036 (2017).
- [27] S. Andersson, B. Collén, U. Kuylenstierna, and A. Magnéli, *Acta Chem. Scand.* **11**, 1641 (1957).
- [28] J. K. Hulm, C. K. Jones, R. A. Hein, and J. W. Gibson, *J. Low Temp. Phys.* **7**, 291 (1972).
- [29] M. G. Kostenko and A. A. Rempel, *Phys. Solid State* **53**, 1909 (2011).
- [30] See Supplemental Material at <http://link.aps.org/supplemental/10.1103/PhysRevB.98.064501> for the structures, compositions, upper critical fields, density of states, and Hall measurements of  $\text{TiO}_x$  films.
- [31] A. Kapitulnik, S. A. Kivelson, and B. Spivak, [arXiv:1712.07215](https://arxiv.org/abs/1712.07215).
- [32] M. Mulligan and S. Raghu, *Phys. Rev. B* **93**, 205116 (2016).
- [33] M. P. A. Fisher, G. Grinstein, and S. M. Girvin, *Phys. Rev. Lett.* **64**, 587 (1990).
- [34] I. F. Herbut, *Phys. Rev. Lett.* **87**, 137004 (2001).
- [35] A. B. Harris, *J. Phys. C* **7**, 1671 (1974).
- [36] J. Biscaras, N. Bergeal, S. Hurand, C. Feuillet-Palma, A. Rastogi, R. C. Budhani, M. Grilli, S. Caprara, and J. Lesueur, *Nat. Mater.* **12**, 542 (2013).
- [37] A. M. Goldman, *Int. J. Mod. Phys. B* **24**, 4081 (2010).
- [38] H. Lei, K. Wang, R. Hu, H. Ryu, M. Abeykoon, E. S. Bozin, and C. Petrovic, *Sci. Technol. Adv. Mater.* **13**, 054305 (2012).
- [39] N. R. Werthamer, E. Helfand, and P. C. Hohenberg, *Phys. Rev.* **147**, 295 (1966).
- [40] G. Fuchs, S. L. Drechsler, N. Kozlova, M. Bartkowiak, J. E. Hamann-Borrero, G. Behr, K. Nenkov, H. H. Klauss, H. Maeter, and A. Amato, *New J. Phys.* **11**, 075007 (2009).
- [41] A. A. Valeeva, A. A. Rempel, W. Sprengel, and H.-E. Schaefer, *Phys. Rev. B* **75**, 094107 (2007).
- [42] M. H. Theunissen and P. H. Kes, *Phys. Rev. B* **55**, 15183 (1997).
- [43] A. V. Samoilov, N. C. Yeh, and C. C. Tsuei, *Phys. Rev. B* **57**, 1206 (1998).
- [44] T. Vojta, A. Farquhar, and J. Mast, *Phys. Rev. E* **79**, 011111 (2009).
- [45] W. E. Pickett, *Rev. Mod. Phys.* **61**, 433 (1989).
- [46] M. D. Segall, P. J. D. Lindan, M. J. Probert, C. J. Pickard, P. J. Hasnip, S. J. Clark, and M. C. Payne, *J. Phys.: Condens. Matter* **14**, 2717 (2002).
- [47] J. P. Perdew, K. Burke, and M. Ernzerhof, *Phys. Rev. Lett.* **77**, 3865 (1996).
- [48] B. Sacépé, T. Dubouchet, C. Chapelier, M. Sanquer, M. Ovia, D. Shahar, M. Feigel'man, and L. Ioffe, *Nat. Phys.* **7**, 239 (2011).
- [49] Z. Yamani and M. Akhavan, *Solid State Commun.* **107**, 197 (1998).
- [50] L. Zhang and Z. J. Tang, *Phys. Rev. B* **70**, 174306 (2004).
- [51] J. Billy, V. Josse, Z. Zuo, A. Bernard, B. Hambrecht, P. Lugan, D. Clément, L. Sanchez-Palencia, P. Bouyer, and A. Aspect, *Nature* **453**, 891 (2008).
- [52] T. Schwartz, G. Bartal, S. Fishman, and M. Segev, *Nature* **446**, 52 (2007).
- [53] X. Liu, C. Zhang, F. X. Hao, T. Y. Wang, Y. J. Fan, Y. W. Yin, and X. G. Li, *Phys. Rev. B* **96**, 104505 (2017).
- [54] H. H. Wen, S. L. Li, Z. W. Zhao, H. Jin, Y. M. Ni, Z. A. Ren, G. C. Che, and Z. X. Zhao, *Phys. C (Amsterdam, Neth.)* **363**, 170 (2001).
- [55] H. Beidenkopf, N. Avraham, Y. Myasoedov, H. Shtrikman, E. Zeldov, B. Rosenstein, E. H. Brandt, and T. Tamegai, *Phys. Rev. Lett.* **95**, 257004 (2005).
- [56] A. K. Pramanik, S. Aswartham, A. Wolter, S. Wurmehl, V. Kataev, and B. Büchner, *J. Phys.: Condens. Matter* **25**, 495701 (2013).
- [57] M. Abdel-Hafiez, X. M. Zhao, A. A. Kordyuk, Y. W. Fang, B. Pan, Z. He, C. G. Duan, J. Zhao, and X. J. Chen, *Sci. Rep.* **6**, 31824 (2016).
- [58] Y. L. Loh, M. Randeria, N. Trivedi, C. C. Chang, and R. Scalettar, *Phys. Rev. X* **6**, 021029 (2016).